



Large kinetic asymmetry in the metal-insulator transition nucleated at localized and extended defects

W. Fan,^{1,2} J. Cao,^{1,3} J. Seidel,³ Y. Gu,⁴ J. W. Yim,^{1,3} C. Barrett,^{1,3} K. M. Yu,³ J. Ji,² R. Ramesh,^{1,3} L. Q. Chen,⁴ and J. Wu^{1,3,*}

¹*Department of Materials Science and Engineering, University of California, Berkeley, Berkeley, California 94720, USA*

²*Department of Thermal Science and Energy Engineering, University of Science and Technology of China, Hefei, China*

³*Materials Sciences Division, Lawrence Berkeley National Laboratory, Berkeley, California 94720, USA*

⁴*Department of Materials Science and Engineering, Pennsylvania State University, University Park, Pennsylvania 16802, USA*

(Received 22 March 2011; published 2 June 2011)

Superheating and supercooling effects are characteristic kinetic processes in first-order phase transitions, and asymmetry between them is widely observed. In materials where electronic and structural degrees of freedom are coupled, a wide, asymmetric hysteresis may occur in the transition between electronic phases. Structural defects are known to seed heterogeneous nucleation of the phase transition, hence reduce the degree of superheating and supercooling. Here we show that in the metal-insulator transition of single-crystal VO₂, a large kinetic asymmetry arises from the distinct spatial extension and distribution of two basic types of crystal defects: point defects and twin walls. Nanometer-thick twin walls are constantly consumed but regenerated during the transition to the metal phase, serving as dynamical heterogeneous nucleation seeds and eliminating superheating. On the other hand, the transition back to the insulator phase relies on nucleation at point defects because twinning is structurally forbidden in the metal phase, leading to a large supercooling. By controlling the formation, location, and extinction of these defects, the kinetics of the phase transition might be externally modulated, offering possible routes toward unique memory and logic device technologies.

DOI: [10.1103/PhysRevB.83.235102](https://doi.org/10.1103/PhysRevB.83.235102)

PACS number(s): 71.30.+h, 72.20.-i, 72.80.Ga

I. INTRODUCTION

Supersaturation is a kinetic phenomenon frequently observed in first-order phase transitions, in which the low-temperature phase persists above the transition temperature (superheating) and the high-temperature phase persists below the transition temperature (supercooling). The degree of superheating is not necessarily equal to that of the supercooling. For example, a large asymmetry exists in melting and crystallization of elemental metals¹ and water.² Asymmetric phase transitions also arise in correlated electron materials where electronic and structural degrees of freedom are coupled, such as asymmetric hysteresis in electric conductivity in VO₂ (Refs. 3 and 4) and NdNiO₃,⁵ and magnetization in Ce(FeRu)₂ (Refs. 6 and 7) and CuMoO₄,⁸ but the microscopic origin remains elusive. Defects are known to seed heterogeneous nucleation of the structural phase transition, and hence reduce the degree of superheating or supercooling. Here we show that a large kinetic asymmetry may arise from the distinct spatial extension and distribution of two basic types of crystal defects: point defects and twin walls. In the structural transition, the low-symmetry structure mimics a higher-symmetry structure at its twin wall.⁹ We show that such a twin wall can act as a catalyst to *dynamically* and *sustainably* nucleate the high-symmetry structure during the transition; in contrast, the transition back to the low-symmetry structure relies on nucleation at point defects. The distinct topology and distribution of twin wall and point defects result in disordered nucleation and coexistence of electronic phases during heating, but long-range phase ordering during cooling.

Our investigation of the large kinetic asymmetry is based on probing the model metal-insulator phase transition (MIT) kinetics in twinned and twin-free single-crystal vanadium dioxide (VO₂) microbeams (MBs). Twin walls of the insulator

phase in VO₂ microplatelets have recently been discovered to undergo a MIT separately from the bulk.^{10,11} The geometry and lattice orientation of our MBs restrict the two phases to coexist one dimensionally along the MB axis.¹² This eliminates the percolation process in MIT in thin films¹³ or frustrated domain structures in platelets,¹⁰ allowing its initial nucleation process to be directly, electrically probed. Strain-free VO₂ undergoes the first-order MIT at $T_C^0 \approx 68^\circ\text{C}$ with a drastic change in conductivity and optical reflection.¹⁴⁻¹⁶ The MIT is accompanied with a structural change from the low-temperature, insulating, monoclinic phase (*M*) to the high-temperature, metallic, tetragonal phase (rutile structure, *R*).¹⁴ It is known that another monoclinic, insulating structure (*M*₂, differentiated from the first *M* phase known as *M*₁) can be induced by uniaxial compression perpendicular to *c*_R (Refs. 14, 15, and 17) or uniaxial tension parallel to *c*_R.^{18,19} The transition from *M*₁ to *R* features a spontaneous strain of -1% (shrinkage along the *c*_R direction), while the spontaneous strain is 0.3% (elongation along *c*_R) across the *M*₁-to-*M*₂ transition.¹⁵ Consequently, according to the Clapeyron equation, uniaxial compression (or tension) along *c*_R drives the *M*₁ structure toward the *R* (or *M*₂) structure.²⁰ It is established that under white-light illumination, both *M*₁ and *M*₂ phases of VO₂ show a brighter optical reflectivity than the *R* phase.¹² This provides a convenient way to identify the phase transition temperature and to image the *M/R* domain structure.

II. EXPERIMENTAL DETAILS

VO₂ MBs were prepared using the vapor transport method reported previously.²¹ During the high-temperature synthesis ($\sim 980^\circ\text{C}$), these MBs crystallize along the *c*_R direction with

$\{110\}_R$ planes as bounding facets on a molten SiO_2 surface. When cooled to lower temperatures, the SiO_2 surface gradually solidifies, mechanically clamping the VO_2 MBs onto the SiO_2 surface. A small percentage of these MBs grow out of the edge of the Si wafer forming long cantilevers, allowing investigation of the MIT in strain-free MBs. For electrical measurement, metal electrodes (15-nm Cr and 400-nm Au) were patterned using standard photolithography and deposited with electron beam evaporation.

Additional bulk point defects were introduced by 3-MeV α -particle irradiation with controlled doses ($0.01\text{--}2 \times 10^{16} \text{ cm}^{-2}$). The irradiation was performed using a 2.13-MeV He^{2+} beam with current between 40 and 150 nA generated by a Pelletron tandem accelerator. The ion beam was defocused to an area of 40 mm^2 to cover the entire sample. Simulations using the stopping and range of ions in matter (SRIM) software predicted that the concentration of defects generated by the ion beam is relatively uniform, and the ions would penetrate the entire thickness of the VO_2 layer, leaving end of range damage in the substrate. Electrical and optical measurements were carried out right after each irradiation experiments to minimize possible aging effects.

III. RESULTS AND DISCUSSION

A. Experimental results

Figure 1(a) shows the temperature (T) dependence of four-probe resistance (R_{MB}) of two types of MB devices: freestanding and substrate clamped. The freestanding devices were fabricated with VO_2 MBs suspended from the substrate.¹² Its R_{MB} shows an abrupt, single jump down at T_{heat} upon heating and another abrupt jump up at T_{cool} upon cooling, consistent with an abrupt change in optical reflection in freestanding MBs. The superheating and supercooling behavior is symmetric, and the hysteresis width between T_{heat} and T_{cool} is $\sim 13^\circ\text{C}$ in these MBs. The clamped devices, in stark contrast,

feature wide and asymmetric $M \rightarrow R$ and $R \rightarrow M$ transitions. The temperature at which R_{MB} finally drops to the R -phase level is raised from T_C^0 to $\sim 97^\circ\text{C}$. This shift in T_C is expected as the clamping induces uniaxial tensile strain along the MBs.¹⁸ What is striking is the *gradual, continuous* decrease in R_{MB} during heating contrasted to the *sudden, large* jump up in R_{MB} during cooling. This drastically asymmetric heating-cooling behavior in clamped VO_2 MBs is consistent with observations from several other groups,^{4,12} but no explanations were given. During heating, R_{MB} initially follows an Arrhenius temperature dependence ($R_{\text{MB}} \propto \exp(E_a/k_B T)$) in the M phase, with $E_a \sim 0.3 \text{ eV}$, consistent with previously reported data.^{4,22} At $T_1 \approx 62^\circ\text{C}$, R_{MB} starts to decrease more rapidly deviating from the Arrhenius dependence, characterized by small steps jumping downward [Fig. 1(b) inset]. This deviation signifies the emergence of the first R domains that reduce the total resistance. As will be shown later, these first R domains always nucleate around the twin walls of the M_1 phase. Unlike in thin films, in the MB geometry these domains span the entire width of the MB and line up one dimensionally along the MB.¹² Therefore, the total MB resistance R_{MB} sensitively reveals the nucleation process of these R domains. Around $T_2 \approx 66^\circ\text{C}$, R_{MB} jumps up slightly, and then continues to decrease gradually until a high temperature $T_3 (\approx 97^\circ\text{C})$, where the entire MB becomes metallic R phase. The upward jump near T_2 is due to the emergence of domains of M_2 phase that are three times more resistive than the original M_1 phase.²⁰ These M_2 domains are induced because when the R domains grow sufficiently long, they impose a strong tensile strain to neighboring M_1 phase along the nanobeam axis direction (c_R), elastically driving it into the M_2 phase. But immediately after that, a further increase in temperature causes more $M_1 \rightarrow R$ and $M_2 \rightarrow R$ transitions, resulting in a monotonic and continuous decrease in total R_{MB} until T_3 . The smooth $R_{\text{MB}}\text{-}T$ curve during heating indicates small or no superheating for the $M \rightarrow R$ transition. In contrast, the large supercooling in the $R \rightarrow M$

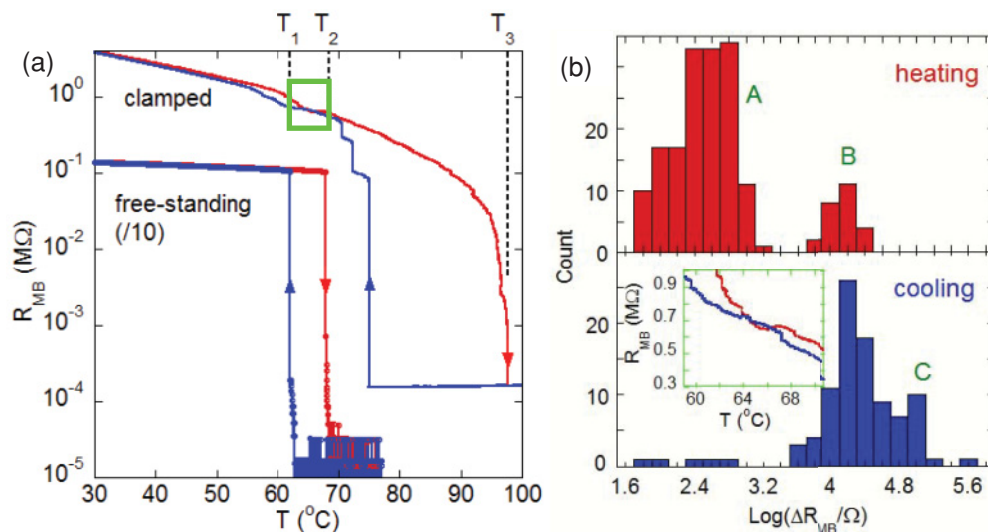


FIG. 1. (Color online) Kinetic asymmetry in the metal-insulator transition of VO_2 . (a) Resistance of a clamped device and a freestanding device measured at a temperature changing rate of $2^\circ\text{C}/\text{min}$. The resistance of the freestanding device is divided by 10 to add a vertical offset for clarity. (b) Distinct distribution of resistance steps on the resistance curve measured from a clamped device. The inset shows a closeup view of the boxed area on the clamped device curve in (a) where ministepts can be seen.

transition indicates that the transition is retarded and limited by nucleation of the M phase.

Numerous ministepts exist on the heating R_{MB} - T curve between T_2 and T_3 . These steps come from growth of the small R domains and reflect the M/R domain wall pinning and depinning process along the MB axial direction, akin to the Barkhausen avalanche associated with magnetic domain growth during magnetization. In percolative VO_2 thin films, the distribution of these steps was quantitatively investigated and self-organized criticality was suggested to explain the behavior.²³ We find that in clamped VO_2 MBs which are effectively a one-dimensional system for the domain dynamics, these ministepts distribute as a broad peak (peak A) between ~ 100 and 1000Ω as shown in Fig. 1(b). The larger R_{MB} steps between T_1 and T_2 distribute as another peak (peak B) $\sim 20 \text{ k}\Omega$, distinctly isolated from peak A. The extremely large jumps during cooling are represented with a distinct peak (peak C) on the ΔR_{MB} distribution, as shown in Fig. 1(b). The isolated distribution of these three peaks reflects that distinct processes are responsible for these ΔR_{MB} steps.

To elucidate the domain nucleation and expansion process, Fig. 2(a) shows an optically imaged domain structure at selected temperatures, which leads to the following conclusions: (i) During heating, the first R domains nucleate at $T_1 \approx 63^\circ\text{C}$ at seemingly random positions; (ii) at higher T , the randomly distributed R domains start to redistribute

correlatively and order themselves; (iii) the random R domain edges make an angle of either $\sim \pm 65^\circ$ or 90° to c_R , but when the R domains are ordered the angle is always 90° ; and most importantly, (iv) during heating the expansion of R domains is smooth and gradual, yet during cooling the M domains emerge abruptly at periodic positions. It has been shown that the one-dimensionally ordered M/R domain structure is caused by energy minimization of the coherently strained MB/ SiO_2 system,^{12,24} where the domain period is determined by a competition between long-range elastic interaction with the SiO_2 surface and the positive M/R domain wall energy. Therefore, the random or ordered distribution of M/R domains signifies a short-range or long-range interaction, respectively, that governs the energetics of domain formation in the system. In the homogeneous nucleation theory, the energy barrier in the MIT of VO_2 is estimated to be $\sim 600 \text{ eV}$ (Ref. 25) based on the M/R domain wall energy¹² and the transition latent heat [$\sim 5 \text{ kJ/mol}$ (Refs. 20 and 26)]; therefore, a homogeneous nucleation is not possible. Hence in both the $M \rightarrow R$ and $R \rightarrow M$ transitions the new phase must nucleate at special sites where the energy barrier is significantly reduced. The long-range interaction is the elastic coupling between the MB and the underneath SiO_2 surface with a characteristic length of the MB thickness ($\sim \mu\text{m}$).²⁴ Therefore, the nucleation sites in the $M \rightarrow R$ transition must distribute with a mean distance comparable to or larger than $\sim \mu\text{m}$ so that they appear random,

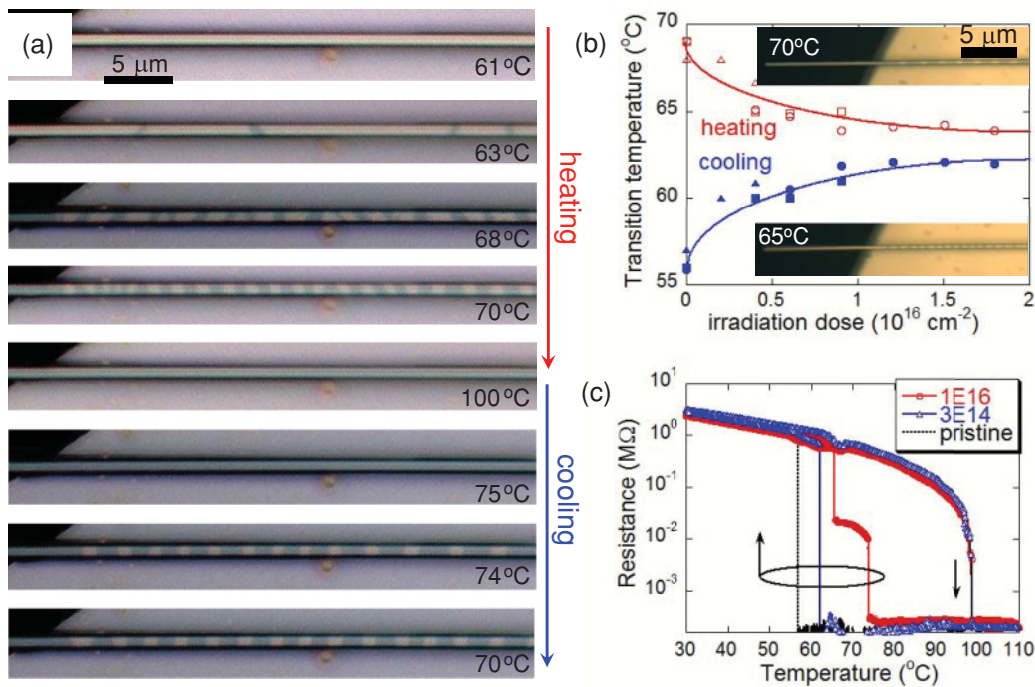


FIG. 2. (Color online) (a) Optical images of an initially M_1 -twinned VO_2 MB recorded during heating and cooling. M and R phases have bright and dark reflections, respectively. The left end of the MB is freestanding. Note the gradual (irregular) domain formation during heating vs abrupt (regular) domain formation during cooling. During cooling the M phase emerges abruptly within $<1^\circ\text{C}$ between 75 and 74°C , and is “born periodic.” (b) Optically determined transition temperatures of freestanding VO_2 as a function of 3-MeV α -particle irradiation dose. Different symbols represent different samples. The curves are a guide to the eye. Inset: Optical image of a freestanding VO_2 MB before and after the MIT. (c) Temperature-dependent four-probe resistance of a clamped device before and after two doses of α -particle irradiation. The superheating is not affected, yet the supercooling is clearly reduced by the irradiation.

whereas in the $R \rightarrow M$ transition they are much smaller than $\sim \mu\text{m}$ so that they are statistically uniform. In the following we show that in the $M \rightarrow R$ transition upon heating, the nucleation sites are the M -phase twin walls. On the other hand, upon cooling, the $R \rightarrow M$ transition nucleates at bulk point defects, because the higher-symmetry, R -phase structure forbids twinning. The point defects have a high density but are not as effective as the twin walls in reducing the homogeneous nucleation barrier. Hence the kinetic asymmetry in the MIT is an intrinsic effect and microscopically originates from the crystal structural asymmetry.

B. Modulating density of point defects

We first explore the role of bulk point defects in the MIT by modulating its density. This was achieved by irradiation with high-energy α particles at controlled doses, a standard method to introduce bulk point defects in semiconductors.²⁷

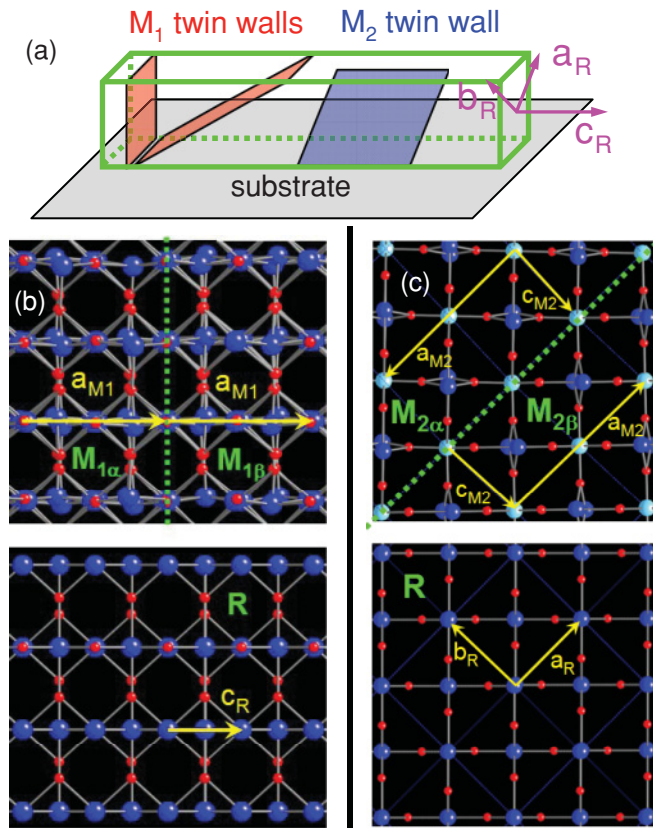


FIG. 3. (Color online) The twin wall structure. (a) A schematic illustrating the orientation of 180° and 90° M_1 twin walls and of 180° M_2 twin wall along a MB. (b) Crystal structure of the 180° twin wall (green dashed line) between two variants of the M_1 phase viewed along the $\pm[011]_{M_1}$ direction, and of the R phase viewed along the same direction ($[1\bar{1}0]_R$). This is the side-view direction of the MB, while the MB length is along the horizontal c_R (or a_{M_1}) direction. A small angle of 0.23° exists between the a_{M_1} axes of the two M_1 variants. (c) Crystal structure of the 180° twin wall (green dashed line) between two variants of the M_2 phase viewed along the $\pm b_{M_2}$ direction, and of the R phase viewed along the same direction (i.e., c_R). This is the direction along the MB length. In (b) and (c), small (red) circles are O atoms, and large (blue and green) circles are V atoms.

We find that in freestanding MBs, the transition temperature T_{heat} is reduced and T_{cool} is nearly symmetrically increased by the irradiation, as shown in Fig. 2(b). In the clamped MBs, in contrast, at irradiation doses that would greatly reduce supersaturation of freestanding MBs, the $R_{\text{MB}}-T$ dependence in the heating half-cycle remains essentially the same, but the supercooling in the cooling half-cycle is clearly reduced by the irradiation [Fig. 2(c)]. Monte Carlo modeling showed that irradiation with 3-MeV α particles at a dose of 10^{16} cm^{-2} would generate native point defects (both vanadium and oxygen vacancies and interstitials) at a density of $\sim 10^{20} \text{ cm}^{-3}$. The α particles all completely penetrate through the micrometer-thick VO_2 and only leave these point defects as damage in the MBs. The fact that T_{heat} and T_{cool} behave nearly symmetrically suggests that the nucleation barrier in the freestanding MBs is comparable for the $R \rightarrow M$ and $M \rightarrow R$ transitions, and bulk point defects play quantitatively the same role in reducing the barrier in both transition directions.

C. Effects of twin walls

Next we investigate the role of twin walls in the MIT. It has been established that both the M_1 (Ref. 11) and M_2 (Ref. 20) phases are easily twinned under strain due to a small energy penalty of the twin walls and a large energy benefit from strain relaxation. In MBs stretched along the axial c_R direction, micro-x-ray diffraction ($\mu\text{-XRD}$)²⁰ and $\mu\text{-Raman}$ ²⁸ show that the MBs are in the M_2 phase and are twinned. In this geometry, only 180° M_2 twin walls are stable, with wall planes in $\{100\}_R$ or $\{010\}_R$ (i.e., $\{001\}_{M_2}$ or $\{00\bar{1}\}_{M_2}$), as shown in Figs. 3(a) and 3(c). On the other hand, in axially compressed MBs the M_1 twin walls may form with two possible orientations.¹¹ The 180° M_1 twin walls lie in the plane of $\{001\}_R$ (i.e., $\{\bar{2}01\}_{M_1}$) perpendicular to c_R , as shown in Figs. 3(a) and 3(b), and the 90° M_1 twin walls lie in the plane of $\{112\}_R$ (i.e., $\{\bar{4}\bar{1}3\}_{M_1}$), making an angle of $\sim 66^\circ$ with c_R . We find that at room temperature, freestanding MBs are always in an untwinned M_1 phase and the substrate clamping mostly causes M_1 twinning. The M_1 twin walls are perpendicular to the MB axis from the top view, and distributed sparsely along the MB. Figure 4(a) shows these M_1 twins imaged with polarized light reflection. The contrast could be due to either 180° or 90° M_1 twins, which the top-view polarized optical microscope cannot differentiate.¹¹ At higher temperatures, a twinned M_2 phase appears with M_2 twin walls parallel to the MB axis and densely packed at a period of $\sim 120 \text{ nm}$, as imaged with a scanning electron microscope (SEM) in Fig. 4(b) and identified with $\mu\text{-XRD}$.²⁰ Considering that the M_2 phase is favored at a tensile strain along c_M ,²⁰ we conclude that high tensile axial strain is developed at higher temperatures ($T \gtrsim T_2$).

It is interesting to note that the first R domains always nucleate around the M_1 -phase twin walls, as shown in Fig. 4(a). The random distribution of these twin walls along the MB results in an irregular and sparse pattern of the initial R domains. Upon a further increase in T , these R domains grow *gradually* and *continuously* along c_R . During this process these R domains reorganize their locations and sizes, and become periodic when the long-range elastic interaction starts

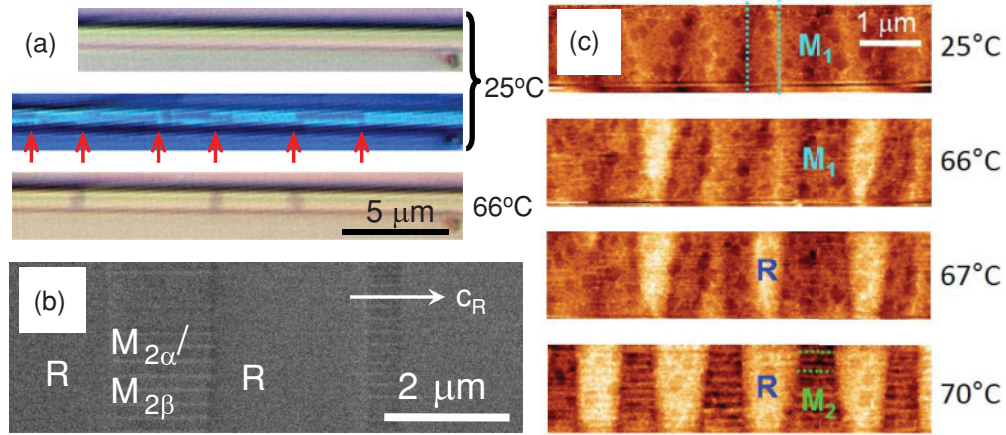


FIG. 4. (Color online) The twin walls as dynamical nucleation sites for the MIT. (a) An optical image (top) and polarized image (middle) of a clamped VO₂ MB showing twinned M_1 domains with twin walls (indicated by arrows) perpendicular to the MB axis, and the nucleation of R domains at some of the twin walls upon heating (bottom). (b) SEM images showing twinned M_2 domains among R domains in a clamped VO₂ beam at 70 °C with M_2 twin walls parallel to the MB axis. (c) Tapping-mode AFM topography images showing $M_{1\alpha}/M_{1\beta}$ twin walls at room temperature. At higher temperatures R domains nucleate at some of the M_1 twin walls. When the R domains are sufficiently large, they induce a twinned M_2 phase in the neighborhood whose twin walls in turn mediate the growth of the R phase. Some of the M_1 twin walls are highlighted by vertical dashed lines in the top image, and some of the M_2 twin walls are highlighted by horizontal dashed lines in the bottom image. The c_R axis is horizontal. Note that the R phase has a larger height than both M_1 and M_2 phases.

to dominate over the short-range domain nucleation. During the cooling process, the first M domains appear *suddenly* at *periodic* positions but only after a large supercooling. It should be noted that the initial M_1 twin walls are localized and completely consumed after the nucleation of first R domains, but the M_2 twin walls are constantly generated during heating. Further growth of the R domains is mediated by M_2 twin walls in the neighboring region, which were induced by tensile strain created by the growth of R domains themselves. A self-sustained $M \rightarrow R$ transition process is thus established, nucleated initially at M_1 twin walls but thereafter mediated *dynamically* by M_2 twin walls. We show the formation of such a complicated $M_1/M_2/R$ domain structure in Fig. 4(c), imaged by an atomic force microscope (AFM), where the different phases can be distinguished by their height and domain periodicity. This is also consistent with the upward jump prior to T_2 in the $R_{MB}-T$ curve in these devices [Fig. 1(a)].

D. Landau theory and phase field modeling

The R domains always nucleate out of the M -phase twin walls (either M_1 or M_2). This is because at the twin walls of the M phases, the crystal structure symmetry is locally elevated and thus mimics structurally the high-symmetry R phase.⁹ In the simplest Ginzburg-Landau theory of first-order ferroelastic phase transition, the free energy can be written as a functional of the order parameter Q ,⁹

$$FQ = \frac{\alpha}{2}Q^2 + \frac{b}{4}Q^4 + \frac{c}{6}Q^6 + \frac{g}{2}\nabla Q^2, \quad (1)$$

where $\alpha(T) = a(T - T_c)$, $a > 0$, $b < 0$, $c > 0$, and $g > 0$.

Across a twin wall at $x = 0$, the well-known solution for Q is obtained by minimizing F ,²⁹

$$Qx = Q_\infty \frac{\sinh x/w}{\sqrt{A + \sinh^2 x/w}}, \quad (2)$$

where $w = \sqrt{g}/(Q_\infty \sqrt{cQ_\infty^2 + b/2})$ is the wall width, and $A = (6cQ_\infty^2 + 3b)/(4cQ_\infty^2 + 3b)$. Q varies from $-Q_\infty$ at $x = -\infty$ to Q_∞ at $x = +\infty$, and vanishes at the wall ($x = 0$). It can be seen that the high-symmetry, paraelastic phase, which is characterized by $Q = 0$, is locally stabilized at the domain wall within a small range of $|x| \lesssim w$.

The transformation strain along the longitudinal direction in the VO₂ MBs is tensile, while along the width direction it is compressive. Therefore, when long-range MB-substrate clamping starts to dominate, domain edge rotation along with domain ordering is energetically favored. To fully simulate the domain structure evolution, a three-dimensional phase field model is necessary. We used a 2-4-6 Landau polynomial to describe the bulk free energy, where the two M_1 variants were described by the two order parameters Q_1 and Q_2 ,

$$F(Q_1, Q_2) = \int_V \left[f(Q_1, Q_2) + \sum_{n=1,2} \frac{\kappa}{2} (\nabla Q_n)^2 + \frac{1}{2} C_{ijkl} \left(\varepsilon_{ij} - \sum_{n=1,2} Q_n^2 \varepsilon_{ij}^{0n} \right) \times \left(\varepsilon_{kl} - \sum_{n=1,2} Q_n^2 \varepsilon_{kl}^{0n} \right) \right] dV, \quad (3)$$

where

$$f(Q_1, Q_2) = \frac{a(T - T_c)}{2} (Q_1^2 + Q_2^2) - \frac{b}{4} (Q_1^4 + Q_2^4) + \frac{c}{6} (Q_1^2 + Q_2^2)^3. \quad (4)$$

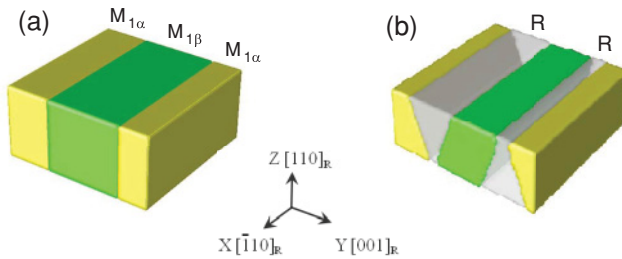


FIG. 5. (Color online) Phase field modeled domains of bottom constrained VO₂. (a) (001)_R twins of the M_1 phase at 25°C. (b) Domain structures after relaxation at 79°C. The M_1 domain edges make an angle of $\sim 65^\circ$ with the c_R direction. The yellow and green colors represent two variants of the M_1 phase. The semitransparent part represents the R phase.

In this formula, a , b , and c are normal Landau coefficients calculated from the transition latent heat. κ is the gradient-energy coefficient obtained from interfacial energy of 50 mJ/m³. C_{ijkl} is the elastic constant which is assumed to be homogeneous inside the VO₂ MBs. Lacking experimental data, our elastic constant for VO₂ came from a first-principles calculation.³⁰ The system is constructed by a substrate at the bottom, a thin film layer in the middle, and a gas phase on the top. For the substrate, we assumed the elastic constant to be isotropic and converted from the Young's modulus of 70 GPa. ε_{ij}^{0n} is the transformation strain (or spontaneous strain) for the n th variant of the R -to- M_1 transition. The mismatch strain was set as $\varepsilon_{22}=0.85\%$ along the longitudinal direction, and all the other strain components were zero. An iteration method developed for an inhomogeneous system was used to obtain the elastic solution.³¹ The parameters in our simulation are $a = 2.98 \times 10^6$ J/m³, $b = 2.06 \times 10^8$ J/m³, $c = 3.35 \times 10^8$ J/m³, $\kappa = 5.2 \times 10^{-12}$ J/m, substrate Young's modulus=70 GPa, substrate Poisson ratio=0.3, $C_{11}=492$ GPa, $C_{22}=407$ GPa, $C_{44}=125$ GPa, $C_{55}=50$ GPa, $C_{12}=161$ GPa, and $C_{13}=32$ GPa. The system starts with (001)_R-oriented M_1 twins at room temperature. After relaxation at 79°C, 10°C higher than the transition temperature, the equilibrium domain structures clearly show two R domains preferentially nucleating at the twin M_1 twin walls, as illustrated in Fig. 5. The domain edges make angles of approximately $\pm 65^\circ$ or 90° to the c_R

direction, consistent with the experimental data. Without these twin walls, the phase transition would rely on point defects to nucleate the new phase, which would result in a high degree of supersaturation.

IV. SUMMARY

In conclusion, we show that in the metal-insulator phase transition in VO₂, two distinct types of structural defects dictate the phase transition kinetics, resulting in a large kinetic asymmetry of the transition. Extended twin walls serve as a catalyst to dynamically and sustainably nucleate the metal phase and thus effectively eliminate superheating, whereas such a benefit is absent in supercooling. Localized point defects nucleate the new phase in the cooling process but much less effectively than the twin walls. This is expected to be a general effect in first-order electronic transitions involving structural changes, as both twin walls and point defects exist ubiquitously in single crystals and epitaxial films of a vast majority of materials. In addition, unlike grain boundaries which are a result of growth, twin walls could be created, displaced, and erased by post-growth processing such as heating or applying external stress;^{11,32} point defects may also be introduced by irradiation and removed by thermal annealing. Therefore, these structural defects potentially offer a unique route to control the kinetics, not merely the thermodynamics, of electronic phase transitions. It can be envisioned that a metal or insulator domain can be preferentially and dynamically nucleated and eliminated at specific locations by controlling the twin wall formation or injecting point defects.

ACKNOWLEDGMENTS

This work was supported by the Laboratory Directed Research and Development Program of Lawrence Berkeley National Laboratory (LBNL) under US Department of Energy Contract No. DE-AC02-05CH11231 (irradiation and measurements), and by the National Science Foundation (NSF) under Grant No. EEC-0832819 (material synthesis and device fabrication), and NSF Grant No. DMR-0820404 (theory and modeling). We gratefully acknowledge discussion with Professor D. Cobden and Professor J. W. Morris. J.S. acknowledges support from the Alexander von Humboldt foundation.

*wuj@berkeley.edu

¹M. Iwamatsu, *J. Phys. Condens. Matter* **11**, L1 (1999).

²O. Mishima and H. E. Stanley, *Nature (London)* **396**, 329 (1998).

³R. A. Aliev and V. A. Klimov, *Phys. Solid State* **46**, 532 (2004).

⁴J. Wei, Z. Wang, W. Chen, and D. H. Cobden, *Nat. Nanotech.* **4**, 420 (2009).

⁵D. Kumar, K. P. Rajeev, J. A. Alonso, and M. J. Martinez-Lope, *J. Phys. Condens. Matter* **21**, 185402 (2009).

⁶M. K. Chattopadhyay, S. B. Roy, A. K. Nigam, K. J. S. Sokhey, and P. Chaddah, *Phys. Rev. B* **68**, 174404 (2003).

⁷A. Haldar, N. K. Singh, Y. Mudryk, K. G. Suresh, A. K. Nigam, and V. K. Pecharsky, *Solid State Commun.* **150**, 879 (2010).

⁸T. Ito, H. Takagi, and T. Asano, *Chem. Mater.* **21**, 3376 (2009).

⁹E. K. H. Salje, *Phase Transitions in Ferroelastic and Co-Elastic Crystals* (Cambridge University Press, Cambridge, UK, 1990).

¹⁰A. Tselev, V. Meunier, E. Strelcov, W. A. Shelton, I. A. Lukyanchuk, K. Jones, R. Proksch, A. Kolmakov, and S. V. Kalinin, *ACS Nano* **4**, 4412 (2010).

¹¹A. Tselev, E. Strelcov, I. A. Lukyanchuk, J. D. Budai, J. Z. Tischler, I. N. Ivanov, K. Jones, R. Proksch, S. V. Kalinin, and A. Kolmakov, *Nano Lett.* **10**, 2003 (2010).

- ¹²J. Wu, Q. Gu, B. S. Guiton, N. de Leon, O. Lian, and H. Park, *Nano Lett.* **6**, 2313 (2006).
- ¹³M. M. Qazilbash *et al.*, *Science* **318**, 1750 (2007).
- ¹⁴V. Eyert, *Ann. Phys. (Berlin)* **11**, 650 (2002).
- ¹⁵M. Marezio, B. McWhan, P. D. Dernier, and J. P. Remeika, *Phys. Rev. B* **5**, 2541 (1972).
- ¹⁶J. C. Rakotoniaina, R. Mokranitamellin, J. R. Gavarri, G. Vacquier, A. Casalot, and G. Calvarin, *J. Solid State Chem.* **103**, 81 (1993).
- ¹⁷J. P. Pouget, H. Launois, J. P. D'Haenens, P. Merenda, and T. M. Rice, *Phys. Rev. Lett.* **35**, 873 (1975).
- ¹⁸J. Cao *et al.*, *Nature Nanotech.* **4**, 732 (2009).
- ¹⁹S. Zhang, J. Y. Chou, and L. J. Lauhon, *Nano Lett.* **9**, 4527 (2009).
- ²⁰J. Cao, Y. Gu, W. Fan, L. Q. Chen, C. Barrett, J. Seidel, K. Chen, N. Tamura, M. Kunz, and J. Wu, *Nano Lett.* **10**, 2667 (2010).
- ²¹B. S. Guiton, Q. Gu, A. L. Prieto, M. S. Gudiksen, and H. Park, *J. Am. Chem. Soc.* **127**, 498 (2005).
- ²²J. Cao, W. Fan, H. Zheng, and J. Wu, *Nano Lett.* **9**, 4001 (2009).
- ²³A. Sharoni, J. G. Ramirez, and I. K. Schuller, *Phys. Rev. Lett.* **101**, 026404 (2008).
- ²⁴A. L. Roytburd, *J. Appl. Phys.* **83**, 239 (1998).
- ²⁵R. Lopez, T. E. Haynes, L. A. Boatner, L. C. Feldman, and R. F. Haglund, *Phys. Rev. B* **65**, 224113 (2002).
- ²⁶C. N. Berglund and H. J. Guggenheim, *Phys. Rev.* **185**, 1022 (1969).
- ²⁷S. X. Li, K. M. Yu, J. Wu, R. E. Jones, W. Walukiewicz, J. W. Ager, W. Shan, E. E. Haller, H. Lu, and W. J. Schaff, *Phys. Rev. B* **71**, 161201 (2005).
- ²⁸A. Jones, S. Berweger, J. Wei, D. H. Cobden, and M. Raschke, *Nano Lett.* **10**, 1574 (2010).
- ²⁹W. Cao and L. E. Cross, *Phys. Rev. B* **44**, 5 (1991).
- ³⁰Y. Gu, J. Cao, J. Wu, and L. Q. Chen, *J. Appl. Phys.* **108**, 083517 (2010).
- ³¹S. Y. Hu and L. Q. Chen, *Acta Mater.* **49**, 1879 (2001).
- ³²E. K. H. Salje and H. Zhang, *Phase Transitions* **82**, 452 (2009).